5. E. Bard, B. Hamelin, R. G. Fairbanks, A. Zindler, *Nature* **345**, 405 (1990).
6. E. Bard *et al.*, *Nature*, **382**, 241 (1996).
7. L. F. Montaggioni *et al*., *Geology* **25**, 555 (1997).
8. Two U/Th ages on *A. palmata* were obtained from near the top of Barbados core RGF-9: 14,690 ± 85 yr B.P. (RGF9-13-3) and 14,230 ± 100 yr B.P. (RGF9-8-2). When the long-term uplift rate of Barbados is accounted for (0.34 m/kyear) (*1*), the difference in elevation between the two samples represents a relative sea-level rise of 5.5 m. However, given the conventional water-depth uncertainty constrained by this species (within 6 m of sea level), a maximum rise in relative sea level of 11.5 m, or more than half the rise associated with mwp-1A, is possible. The youngest dated sample of *A. palamata* (RGF9-8-2) is overlain by deep-water species *Porites astroides* and *A. cervicornis*, suggesting that the 14,230 kyr B.P. horizon was already in the process of drowning in response to rapidly rising sea level. This sample may thus have been well below its normal 6-m water-depth tolerance at the time it grew, allowing more than 11.5 m of relative sea-level rise since 14,690 ± 85 yr B.P.
9. T. Hanebuth, K. Stattegger, P. M. Grootes, *Science* **288**, 1033 (2000).
10. K. A. Hughen, J. R. Southon, S. J. Lehman, J. T. Overpeck, *Science* **290**, 1951 (2000).
11. H. Kitigawa, J. van der Plicht, *Radiocarbon* **42**, 369 (2000).
12. P. U. Clark, N. G. Pisias, T. F. Stocker, A. J. Weaver, *Nature* **415**, 863 (2002).
13. M. Kienast, T. J. J. Hanebuth, C. Pelejero, S. Steinke, *Geology* **31**, 67 (2003).
14. A. J. Weaver *et al*., *Atmosphere-Ocean* **39**, 361 (2001).
15. The model consists of a three-dimensional (3D) ocean general circulation model (GCM) coupled to a thermodynamic-dynamic sea ice model and an energy-moisture balance atmosphere model. A reduced-complexity atmosphere model is used for computational efficiency. Atmospheric heat transport is parameterized through Fickian diffusion, and moisture transport is accomplished through both advection and diffusion, with precipitation occurring when the relative humidity exceeds 85%. The atmospheric dynamical feedback option has not been included in this application. Precipitation over land instantaneously returns to the ocean via 1 of 33 river basins unless it falls as snow, in which case it is locally retained until it melts. The atmospheric model includes a parameterization of water vapor–planetary longwave feedbacks, although the radiative forcing associated with changes in atmospheric CO_2 is externally imposed as a reduction of the planetary long-wave radiative flux. The ocean component of the coupled model is a fully nonlinear 3D ocean GCM with a global resolution of 3.6° (zonal) by 1.8° (meridional) and 19 vertical levels. It includes the parameterization of Gent and McWilliams to represent the effect of mixing associated with mesoscale eddies. The sea-ice model incorporates an elastic-viscous-plastic rheology representation of dynamics, a two-category thickness distribution, and ice-snow thermodynamics. The model resolves the annual cycle, and the incoming solar radiation at the top of the atmosphere depends on the orbital parameters. One of the virtues of the coupled model is that we do not need to use explicit flux adjustments to keep the simulation of the present climate stable.
16. O. A. Saenko, A. Schmittner, A. J. Weaver, *J. Phys. Oceanogr.* **32**, 3376 (2002).
17. A. Schmittner, K. J. Meissner, M. Eby, A. J. Weaver, *Paleoceanogr.* **17** (**2**), 1015, doi:10.1029/2001PA-000633 (2002).
18. A. Schmittner, M. Yoshimori, A. J. Weaver, *Science* **295**, 1489 (2002).
19. S. Manabe, R. J. Stouffer, *Tellus* **51A**, 400 (1999).
20. S. Rahmstorf, *Clim. Dyn.* **12**, 799 (1996).
21. A. J. Weaver, *Geophys. Monogr. Am. Geophys. Union* **112** (American Geophysical Union, Washington, DC, 1999), pp. 285–300.
22. R. B. Alley, P. U. Clark, *Ann. Rev. Earth Planet. Sci.* **27**, 149 (1999).
23. T. F. Stocker, D. G. Wright, *Nature* **351**, 729 (1991).
24. A. F. Fanning, A. J. Weaver, *Paleoceanogr.* **12**, 307 (1997).
25. E. Maier-Reimer, U. Mikolajewicz, in *Oceanography*, A. Ayala-Castanares, W. Wooster, A. Yanez-Arancibia, Eds. (Universidad Nacional Autónoma de México Press, Mexico City, Mexico, 1989), pp. 87–99.
26. A. Schiller, U. Mikolajewicz, R. Voss, *Clim. Dyn.* **13**, 325 (1997).
27. S. Manabe, R. J. Stouffer, *Paleoceanogr.* **12**, 321 (1997).
28. U. Mikolajewizc, *Ann. Glaciol.* **27**, 311 (1998)
29. D. Seidov, B. J. Haupt, E. J. Barron, M. Maslin, *Geophys. Monogr. Am. Geophys. Union* **126** (American Geophysical Union, Washington, DC, 2001), pp. 147–168.
30. M. H. England, J. S. Godfrey, A. C. Hirst, M. Tomczak, *J. Phys. Oceanogr.* **23**, 1553 (1993).
31. M. S. McCartney, *Deep-Sea Res.* **24**, 103 (1977).
32. O. A. Saenko, A. J. Weaver, M. H. England, *J. Phys. Oceanogr.*, in press.
33. H. M. Stommel, *Tellus* **13**, 224 (1961).
34. T. Blunier, E. J. Brook, *Science* **291**, 109 (2001).
35. E. Monnin *et al*., *Science* **291**, 112 (2001).
36. W. S. Broecker *et al*., *Nature* **341**, 318 (1989).
37. P. U. Clark *et al*., *Science* **293**, 283 (2001).
38. E. Bard, M. Arnold, R. G. Fairbanks, B. Hamelin, *Radiocarbon* **35**, 191 (1993).
39. E. Bard, F. Rostek, J.-L. Turon, S. Gendreau, *Science* **289**, 1321 (2000).
40. P. M. Grootes, M. Stuiver, J. W. C. White, S. J. Johsen, J. Jouzel, *Nature* **366**, 552 (1993).
41. M. Stuiver, P. M. Grootes, *Quat. Res.* **53**, 277 (2000).
42. Y. Yokoyama, K. Lambeck, P. De Deckker, P. Johnston, K. Fifield, *Nature* **406**, 713 (2000).
43. R. L. Edwards, H. Cheng, M. T. Murrell, S. J. Goldstein, *Science* **260**, 962 (1993).

44. We are grateful for funding from the Natural Sciences and Engineering Research Council via the operating and Climate System History and Dynamics programs and for research support from the Canadian Foundation for Climate and Atmospheric Sciences. This research was also made possible through support from the Killam Foundation and the Canada Research Chair program to A.J.W. and from the Earth System History Program of NSF to P.U.C. We also acknowledge discussions with J. Gregory and M. Kienast and are grateful for the insightful comments of two anonymous reviewers.

2 December 2002; accepted 28 January 2003

Spread of HTLV-I Between Lymphocytes by Virus-Induced Polarization of the Cytoskeleton

Tadahiko Igakura,[1,3] Jane C. Stinchcombe,[4] Peter K. C. Goon,[1] Graham P. Taylor,[2] Jonathan N. Weber,[2] Gillian M. Griffiths,[4] Yuetsu Tanaka,[5] Mitsuhiro Osame,[3] Charles R. M. Bangham[1]*

Cell contact is required for efficient transmission of human T cell leukemia virus–type 1 (HTLV-I) between cells and between individuals, because naturally infected lymphocytes produce virtually no cell-free infectious HTLV-I particles. However, the mechanism of cell-to-cell spread of HTLV-I is not understood. We show here that cell contact rapidly induces polarization of the cytoskeleton of the infected cell to the cell-cell junction. HTLV-I core (Gag protein) complexes and the HTLV-I genome accumulate at the cell-cell junction and are then transferred to the uninfected cell. Other lymphotropic viruses, such as HIV-1, may similarly subvert normal T cell physiology to allow efficient propagation between cells.

The human T cell leukemia virus–type 1 (HTLV-I) is an oncogenic exogenous retrovirus that infects between 10 and 20 million people worldwide. Of these infected individuals, 2 to 3% develop adult T cell leukemia/lymphoma (*1*), and a further 2 to 3% develop a variety of chronic inflammatory syndromes, most notably HTLV-I–associated myelopathy/tropical spastic paraparesis (HAM/TSP) (*2*, *3*).

HTLV-I is transmitted between individuals by transfer of infected lymphocytes in breast milk, semen, or blood (*4*). Transfusion with cell-free blood products appears to carry a negligible risk of HTLV-I infection (*5*) . In vitro, efficient spread of HTLV-I infection also requires cell contact (*6*, *7*). Cell contact is required because lymphocytes naturally infected with HTLV-I produce very few cell-free HTLV-I virions and because, of the virions that are released, only 1 in 10^5 to 10^6 is infectious (*8*, *9*).

The mechanism of cell-to-cell spread of HTLV-I is not understood. HTLV-I expresses a surface glycoprotein, the envelope (Env) protein, which is required for infectivity (*9*) and for cell-cell fusion and syncytium formation (*10*–*12*). Env is presumed to bind to a cellular receptor for HTLV-I, but the receptor has not yet been identified (*13*, *14*). Certain integrins, including intercellular and vascular cell-adhesion molecules ICAM-1, ICAM-3, and VCAM, act as cofactors for HTLV-I–induced cell fusion (*15*, *16*).

In this study we tested the hypothesis that HTLV-I is transmitted directly across the cell-cell junction. We used confocal microscopy to examine the distribution of HTLV-I Gag and Env proteins and the HTLV-I genome in fresh, unstimulated peripheral blood mononuclear cells (PBMCs) isolated directly from

[1]Department of Immunology, [2]Department of Genito-Urinary Medicine and Communicable Diseases, Imperial College London, St. Mary's Campus, Norfolk Place, London W2 1PG, UK. [3]The Third Department of Internal Medicine, Faculty of Medicine, Kagoshima University, 8-35-1 Sakuragaoka, Kagoshima 890-8520, Japan. [4]Sir William Dunn School of Pathology, University of Oxford, Oxford OX1 3RE, UK. [5]Department of Infectious Disease and Immunology, Okinawa-Asia Research Center of Medical Science, Faculty of Medicine, University of the Ryukyus, Uehara-cho 207, Nishihara, Okinawa 903-0215, Japan.

*To whom correspondence should be addressed. E-mail: c.bangham@imperial.ac.uk

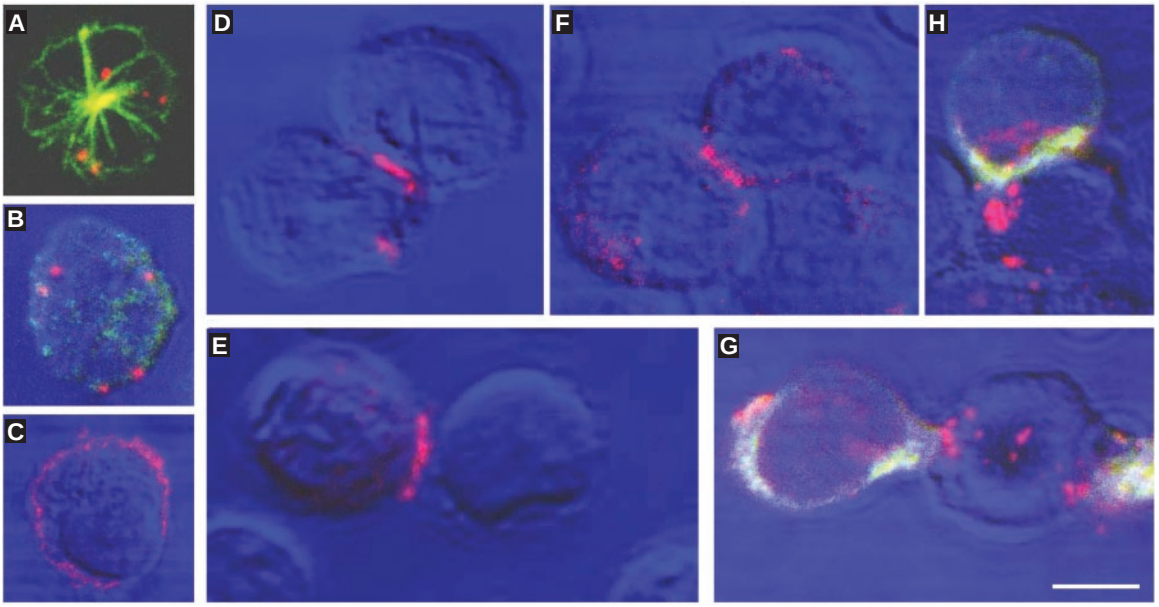

Fig. 1. HTLV-I Gag and Env proteins are unpolarized in an isolated T cell, but accumulate at the cell-cell junction within 40 min of cell contact; Gag protein is transferred from HTLV-I–infected T cells to uninfected T cells within 120 min. (**A** to **C**) Single confocal sections showing isolated $CD4^+$ T cells from a patient with HAM/TSP. (A) $CD4^+$ T cell, tubulin-alpha (green) and Gag p19 (red). (B) $CD4^+$ T cell, tubulin-alpha (green), Gag p15 (red). (C) $CD4^+$ T cell, Env gp46 (red). (**D** to **F**) Confocal images showing polarization of HTLV-I Gag and Env proteins to the cell-cell junction. Conjugates were allowed to form for 40 min between fresh $CD4^+$ T cells from a patient with HAM/TSP. (D) $CD4^+$ T cell, Gag p15 (red). (E) $CD4^+$ T cell, Gag p19 (red). (F) $CD4^+$ T cell, Env gp46 (red). (**G** and **H**) Confocal images showing transfer of Gag p19 protein from HTLV-I–infected T cells to uninfected T cells. Conjugates were allowed to form for 120 min. (G) HTLV-I–infected $CD4^+$ and normal $CD4^+$ T cell, Gag p19 (red). (H) HTLV-I–infected $CD8^+$ and normal $CD4^+$ T cell, Gag p19 (red). HTLV-I–infected T cells were marked with carboxyfluorescein succinimidyl ester (CFSE) (green). The transmission picture [(B) to (H) blue] is superimposed on a 0.4-μm confocal fluorescence single section [(C) to (F) red, (B), (G), and (H) red and green]. Scale bar, 5 μm.

HTLV-I–infected individuals and fixed and stained within 24 hours. We conclude that HTLV-I subverts normal T cell physiology to spread efficiently between host cells, without the need to release cell-free virus particles.

Polarization of virus proteins and nucleic acids. In isolated lymphocytes, we observed clusters of Gag p19- and p15-staining material, predominantly near the cell membrane, as previously described (*17*) (Fig. 1, A and B; fig. S1, a and d). Env gp46 staining appeared uniformly on the cell surface (Fig. 1C). When T cells were allowed to form conjugates with neighboring cells, within 40 min there was strong polarization to the area of cell-cell contact of both Gag protein (Fig. 1, D and E) and Env protein (Fig. 1F).

The adhesion molecule talin accumulated at the cell-cell junction in conjugates containing HTLV-I–infected T cells and formed a ring in about 35% of cases (Fig. 2, B and C; fig. S2, a to c), or a single patch (about 60% of cases) or multiple patches (5%). HTLV-I Gag protein accumulated either in the central talin-free domain (Fig. 2, B and C; fig. S2, a and b) or as clusters overlying or adjacent to talin patches. This accumulation of Gag protein in the center of the cell-to-cell junction was observed in conjugates between $CD4^+$ and $CD4^+$ T cells (Fig. 2, B and C), $CD4^+$ and $CD8^+$ T cells (fig. S2a), and $CD8^+$ and $CD8^+$ T cells. The presence in these accumulations of nucleocapsid staining (p15) (Figs. 1D and 2A) is significant because the nucleocapsid binds the retroviral genome and incorporates it into the virion (*18*).

When $CD4^+$ or $CD8^+$ T cells isolated from a HAM/TSP patient were allowed to form conjugates with T cells from a healthy uninfected donor for 120 min, in addition to accumulation of Gag p19 staining at the cell-cell junction, there was frequent Gag p19 staining in the cells derived from the uninfected donor (Fig. 1, G and H). We observed transfer of Gag p19 staining from $CD4^+$ T cells and $CD8^+$ T cells to both $CD4^+$ and $CD8^+$ allogeneic T cells. This process may represent the initial establishment of HTLV-I infection in a newly infected individual, which involves contact between allogeneic lymphocytes.

Polarization of Gag complexes to the cell-cell junction and transfer to the uninfected cell were also observed in conjugates between $CD4^+$ T cells and both B cells (fig. S1, b and c) and NK cells (fig. S1, e and f).

We used an antisense peptide nucleic acid (PNA) probe in fluorescence in situ hybridization (FISH) to detect the (plus sense) HTLV-I genome, which is normally bound to the Gag polyprotein during retroviral particle formation. The PNA probe stained the HTLV-I producer cell line MT-2 (Fig. 3D). In conjugates formed between MT-2 cells, HTLV-I nucleic acid accumulated at the cell-cell junctions. Uninfected Jurkat cells (Fig. 3C) were not stained. A plus-sense PNA probe, corresponding to the same 15 nucleotides in the HTLV-I Gag gene, was also used as a negative control. In isolated T cells that were naturally infected with HTLV-I, the viral nucleic acid was not polarized (Fig. 3A). However, in two-cell conjugates, the HTLV-I genome accumulated at the cell-to-cell contact area (Fig. 3B); when there, it resembled the polarization of Gag and Env proteins (Fig. 1, D and E). After a 120-min incubation, HTLV-I RNA was transferred from HTLV-I–infected cell to uninfected cell (Fig. 3, E and F), like the Gag protein (Fig. 1, G and H).

Reorientation of microtubule organizing center. We observed frequent reorientation of the microtubule organizing center (MTOC) to the area of cell-cell contact in lymphocyte conjugates (Fig. 2D; fig. S2, d and e): in each case the MTOC lay immediately adjacent to the accumulation of HTLV-I Gag protein. This close apposition of polarized Gag molecules to the MTOC suggested that the microtubule cytoskeleton affected the polarization of Gag. In $CD4^+$-$CD4^+$ T cell conjugates, treatment with 33 nM nocodazole for 90 min blocked the polarization and transfer of Gag protein, both in the absence (Fig. 2, E and F) and the presence (Fig. 2G) of the T cell activator phytohemagglutinin-L (leucoagglutinin, PHA-L). These results suggest that microtubules are involved in transporting Gag-containing material toward the cell-cell junction before transfer into the recipient cell.

Binding of the T cell receptor (TCR) to the major histocompatibility complex (MHC) and the antigen on the surface of another cell causes reorientation of the responding T cell's MTOC to the cell-cell junction. Surprisingly, there was a significant association between MTOC polarization and CD4 positivity in conjugates between autologous $CD4^+$ and $CD8^+$ T cells from

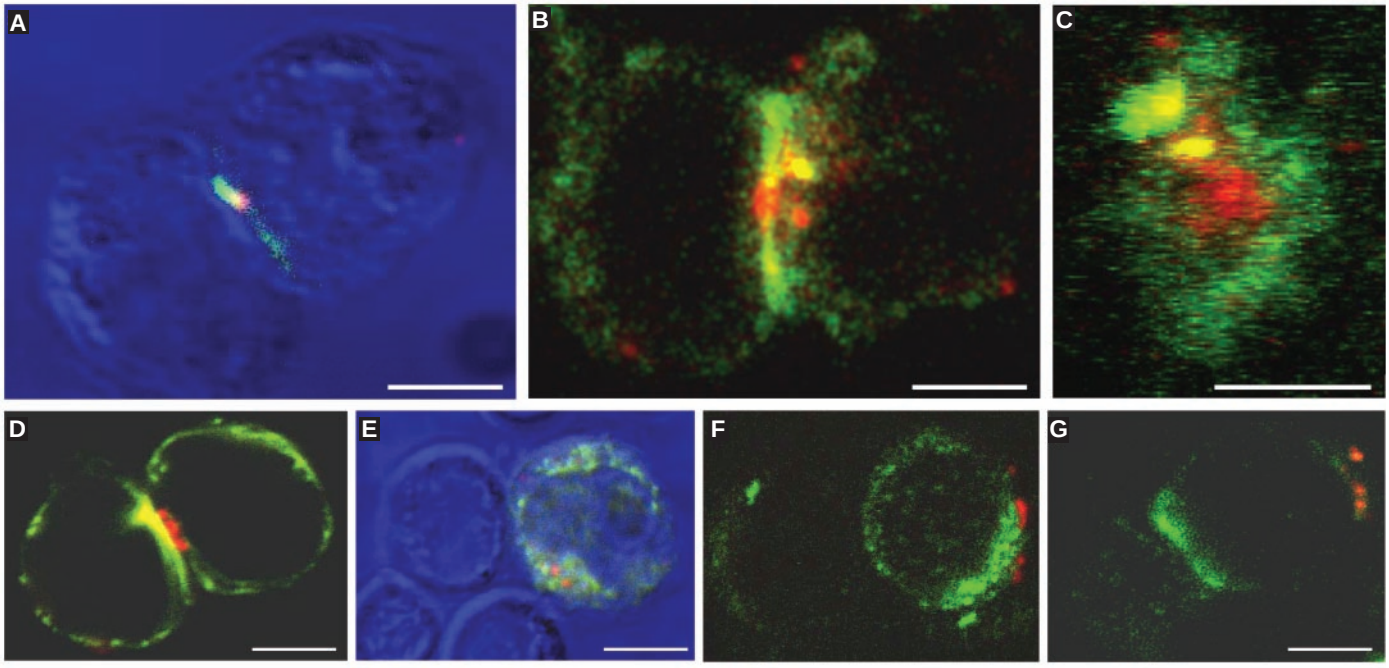

Fig. 2. (**A** to **C**) HTLV-I Gag protein and talin accumulate in distinct domains at the cell-cell junction. Conjugates were allowed to form for 40 min between fresh cells from a HAM/TSP patient. (A) $CD4^+$ T cell conjugate, talin (green), Gag p15 (red). [(B) and (C)] $CD4^+$ T cell conjugate, talin (green), and Gag p19 (red). (C) Z-axis image reconstruction from (B), talin (green), and Gag p19 (red). (**D** to **G**) The MTOC lies adjacent to the polarized HTLV-I Gag protein at the cell-cell junction; however, treatment with nocodazole, an inhibitor of tubulin polymerization, blocks both the polarization to the cell-cell junction and cell-cell transfer of Gag protein. (D) $CD4^+$ T cell conjugate, tubulin-alpha (green), HTLV-I Gag p19 (red). (E) Conjugate between HTLV-I–infected $CD4^+$ T cell labeled with CFSE (green) and normal $CD4^+$ T cell, HTLV-I Gag p19 (red). (F) Autologous $CD4^+$ T cell conjugate, tubulin-alpha (green), HTLV-I Gag p19 (red). (G) Autologous $CD4^+$ T cell conjugate, formed in the presence of PHA-L, talin (green), HTLV-I Gag p19 (red). [(E) to (G)] Treatment with nocodazole. The transmission picture [(A) and (E) blue] is superimposed on a 0.4-μm confocal fluorescence single section (red and green). Scale bars, 5 μm.

an infected individual ($P = 0.046$, Fisher's exact test). This observation raised the possibility that the MTOC polarization was associated with HTLV-I infection of the T cell and was not triggered by antigen recognition.

To test this possibility, we counted the orientation patterns of MTOCs in 304 spontaneous two-cell conjugates formed between fresh $CD4^+$ T cells from two HTLV-I–infected subjects and one uninfected control. The results (table S1) showed a strong association between Gag p19 positivity and MTOC polarization to the cell junction in the same cell. The odds ratio of MTOC polarization in a Gag $p19^+$ cell, compared with a Gag $p19^-$ cell, was 4.07 (95% confidence interval, 3.07 to 5.39; $\chi^2 = 99$; $P \ll 0.001$).

Thus, MTOC polarization in a $CD4^+$ T cell was not triggered by TCR-mediated recognition of HTLV-I antigens presented by the other (infected) T cell: rather, the polarization occurred inside the infected T cell. HTLV-I infection of a T cell apparently induced the cytoskeletal rearrangement that occurred when the HTLV-I–infected T cell made contact with another cell.

Our observations do not rule out other pathways of cell-to-cell spread of HTLV-I, including a contribution from infectious cell-free virions. However, infection by cell-free HTLV-I particles in vitro is very inefficient (*8*, *9*). HTLV-I has retained a functional envelope protein, which is required for infectivity and for HTLV-I–induced cell-cell fusion (*9*, *10*). Clarification of the precise roles of HTLV-I Env in cell-to-cell transmission awaits identification of the cellular receptor(s) and electron microscopic studies of the membrane contact area between the cells. It is possible that the critical role of HTLV-I Env protein is to cause fusion of the two cell membranes (*10*).

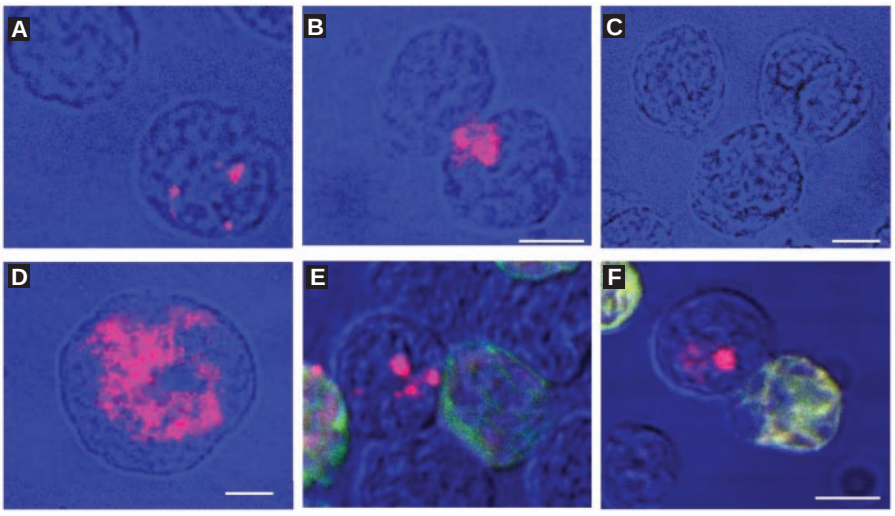

Fig. 3. The HTLV-I genome accumulates at the cell-cell junction and is then transferred to the uninfected cell. (**A** to **D**) Conventional fluorescence images showing plus-strand HTLV-I nucleic acid by PNA-FISH and transmission picture (blue). (**E** and **F**) Confocal images showing plus-strand HTLV-I nucleic acid by PNA-FISH and transmission picture (blue). [(A), (B), and (D) to (F)] HTLV-I nucleic acid (red). [(A) and (B)] $CD4^+$ T cell from HAM/TSP patient, conjugation time 40 min. (C) Jurkat cell (negative control), conjugation time 40 min. (D) MT2 cell (positive control). [(E) and (F)] $CD4^+$ T cell from HAM/TSP patient (marked green with CFSE) and control (uninfected) $CD4^+$ T cell, conjugation time 120 min. Scale bars, 5 μm.

Initiation of polarization. Two factors appeared to be necessary to initiate the observed polarization of the cytoskeleton: HTLV-I infection of the cell and contact with another cell. It is not yet clear which molecules mediate these signals. HTLV-I Env protein is again a candidate for this function, because it is the only HTLV-I protein that is expressed intact on the outside of the infected cell. However, HTLV-I also up-regulates expression of certain adhesion molecules such as integrins (*19*, *20*), which will increase the likelihood of cell-cell adhesion. Furthermore, Yamamoto *et al*. (*20*) found that ligation of ICAM-1 on the cell surface induces expression of HTLV-I genes, which suggests the existence of a positive feedback loop between cell-cell adhesion and HTLV-I gene expression (fig. S3).

HTLV-I Gag protein, in complex with the HTLV-I genome, appears to be transported to the MTOC by a microtubule-dependent process. Microtubules have been shown to be involved in the intracellular transport of other viruses, e.g., adenovirus and herpesvirus (*21*–*23*).

The junction formed between an HTLV-I–infected T cell and another T cell shared two similarities—ordered talin domains and MTOC polarization—with the "immunological synapse" (*24*). However, in the present study the MTOC polarization occurred within the HTLV-I–infected cell, not toward the infected cell. Therefore, MTOC polarization was not triggered by recognition of HTLV-I antigens presented by a neighboring T cell, and the structures we report here cannot be considered an "immunological" synapse. The term "virological synapse" may be more appropriate.

HTLV-I can infect almost any mammalian cell in vitro, but in vivo it is almost confined to T cells, for unknown reasons (*25*–*27*). It is possible that T cell–specific factors are required either for efficient HTLV-I replication or for the process of cell-to-cell transfer reported here.

We conclude that HTLV-I exploits the normal physiology of the T cell to enable efficient cell-to-cell transmission by forming a close contact with the recipient cell and using the cytoskeleton to propel viral material into the recipient cell (fig. S3). Although HTLV-I has a peculiarly strong dependence on cell contact for efficient transmission of the virus between cells, it is possible that other lymphotropic viruses, such as HIV-1 (*28*, *29*), use a similar mechanism to spread between lymphocytes.

References and Notes

1. T. Uchiyama, J. Yodoi, K. Sagawa, K. Takatsuki, H. Uchino, *Blood* **50**, 481 (1977).
2. A. Gessain *et al.*, *Lancet* **2**, 407 (1985).
3. M. Osame *et al.*, *Lancet* **1**, 1031 (1986).
4. N. E. Mueller, W. A. Blattner, in *Viral Infections of Humans: Epidemiology and Control*, A. S. Evans, R. Kaslow, Eds. (Plenum Medical Press, New York, 1997), pp. 785–813.
5. K. Okochi, H. Sato, Y. Hinuma, *Vox Sang* **46**, 245 (1984).
6. N. Yamamoto, M. Okada, Y. Koyanagi, M. Kannagi, Y. Hinuma, *Science* **217**, 737 (1982).
7. M. Popovic *et al.*, *Science* **219**, 856 (1983).
8. N. Fan *et al.*, *J. Clin. Microbiol.* **30**, 905 (1992).
9. D. Derse, S. A. Hill, P. A. Lloyd, H. Chung, B. A. Morse, *J. Virol.* **75**, 8461 (2001).
10. L. Delamarre, A. R. Rosenberg, C. Pique, D. Pham, M. C. Dokhelar, *J. Virol.* **71**, 259 (1997).
11. K. Nagy, P. Clapham, R. Cheingsong-Popov, R. A. Weiss, *Int. J. Cancer* **32**, 321 (1983).
12. S. R. Jassal, M. D. Lairmore, A. J. Leigh-Brown, D. W. Brighty, *Virus Res.* **78**, 17 (2001).
13. M. A. Sommerfelt *et al.*, *Science* **242**, 1557 (1988).
14. S. R. Jassal, R. G. Pohler, D. W. Brighty, *J. Virol.* **75**, 8317 (2001).
15. J. E. Hildreth, A. Subramanium, R. A. Hampton, *J. Virol.* **71**, 1173 (1997).
16. S. Daenke, S. A. McCracken, S. Booth, *J. Gen. Virol.* **80**, 1429 (1999).
17. I. Le Blanc *et al.*, *J. Virol.* **76**, 905 (2002).
18. C. Meric, P. F. Spahr, *J. Virol.* **60**, 450 (1986).
19. H. Valentin *et al.*, *J. Virol.* **71**, 8522 (1997).
20. A. Yamamoto, H. Hara, T. Kobayashi, *J. Neurol. Sci.* **151**, 121 (1997).
21. B. R. Cullen, *Cell* **105**, 697 (2001).
22. M. Suomalainen, M. Y. Nakano, K. Boucke, S. Keller, U. F. Greber, *EMBO J.* **20**, 1310 (2001).
23. H. Mabit *et al.*, *J. Virol.* **76**, 9962 (2002).
24. A. Grakoui *et al.*, *Science* **285**, 221 (1999).
25. K. Nagy, R. A. Weiss, P. R. Clapham, R. Cheinsong-Popov, in *Human T-Cell Leukemia/Lymphoma Viruses*, R. C. Gallo, Ed. (Cold Spring Harbor Laboratory Press, Cold Spring Harbor, NY, 1984), pp. 121–131.
26. J. H. Richardson, A. J. Edwards, J. K. Cruickshank, P. Rudge, A. G. Dalgleish, *J. Virol.* **64**, 5682 (1990).
27. E. Hanon *et al.*, *Immunity* **13**, 657 (2000).
28. D. S. Dimitrov *et al.*, *J. Virol.* **67**, 2182 (1993).
29. R. Pearce-Pratt, D. Malamud, D. M. Phillips, *J. Virol.* **68**, 2898 (1994).

30. We thank the staff and patients of St. Mary's Hospital for their cooperation, Q. Sattentau and D. M. Davis (Imperial College, UK) for helpful discussions, A. Barnard for help with the MTOC orientation experiments, and N. White (Sir William Dunn School of Pathology, University of Oxford, UK) for help with the use of the confocal microscope facility. This work was supported by The Wellcome Trust (UK).

Supporting Online Material

www.sciencemag.org/cgi/content/full/1080115/DC1
Materials and Methods
Figs. S1 to S3
Table S1
References

4 November 2002; accepted 28 January 2003
Published online 13 February 2003;
10.1126/science.1080115
Include this information when citing this paper.

REPORTS

Grain Boundary Scars and Spherical Crystallography

A. R. Bausch,[1]* M. J. Bowick,[2]* A. Cacciuto,[3] A. D. Dinsmore,[4] M. F. Hsu,[5] D. R. Nelson,[5] M. G. Nikolaides,[1,5] A. Travesset,[6] D. A. Weitz[5]

We describe experimental investigations of the structure of two-dimensional spherical crystals. The crystals, formed by beads self-assembled on water droplets in oil, serve as model systems for exploring very general theories about the minimum-energy configurations of particles with arbitrary repulsive interactions on curved surfaces. Above a critical system size we find that crystals develop distinctive high-angle grain boundaries, or scars, not found in planar crystals. The number of excess defects in a scar is shown to grow linearly with the dimensionless system size. The observed slope is expected to be universal, independent of the microscopic potential.

Spherical particles on a flat surface pack most efficiently in a simple lattice of triangles, similar to the arrangement of billiard balls at the start of a game. Such six-fold coordinated triangular lattices (*1*) cannot, however, be wrapped on the curved surface of a sphere; instead, there must be extra defects in coordination number. Soccer balls and C_{60} fullerenes (*2*, *3*) provide familiar realizations of this fact; they have 12 pentagonal panels and 20 hexagonal panels. The necessary packing defects can be characterized by their topological or disclination charge, q, which is the departure of their coordination number c from the preferred flat space value of 6 ($q = 6 - c$); a classic theorem of Euler (*4*, *5*) shows that the total disclination charge of any triangulation of the sphere must be 12 (*6*). A total disclination charge of 12 can be achieved in many ways, however, which makes the determination of the minimum-energy configuration of repulsive particles, essential for crystallography on a sphere, an extremely difficult problem. This difficulty was recognized nearly 100 years ago by J. J. Thomson (*7*), who attempted, unsuccessfully, to explain the periodic table in terms of rigid electron shells. Similar problems recur in fields as diverse as multielectron bubbles in superfluid helium (*8*), virus morphology (*9*–*11*), protein s-layers (*12*, *13*), and coding theory (*14*, *15*). Indeed, both the classic

Spread of HTLV-I Between Lymphocytes by Virus-Induced Polarization of the Cytoskeleton

Tadahiko Igakura, Jane C. Stinchcombe, Peter K. C. Goon, Graham P. Taylor, Jonathan N. Weber, Gillian M. Griffiths, Yuetsu Tanaka, Mitsuhiro Osame and Charles R. M. Bangham (February 13, 2003)

Science **299** (5613), 1713-1716. [doi: 10.1126/science.1080115]
originally published online February 13, 2003

Editor's Summary

Science (print ISSN 0036-8075; online ISSN 1095-9203) is published weekly, except the last week in December, by the American Association for the Advancement of Science, 1200 New York Avenue NW, Washington, DC 20005.